JOURNAL OF SOLID STATE CHEMISTRY 102, 446–454 (1993)

Single-Crystal Electrical Resistivities of Some Ta-Rich Chalcogenides

KYUNGSOO AHN AND TIMOTHY HUGHBANKS[1]

Department of Chemistry, Texas A&M University, College Station, Texas 77843-3255

Received March 23, 1992; in revised form July 9, 1992; accepted July 14, 1992

Vapor phase transport synthesis of several Ta-rich chalcogenides affords us good single crystals for four-probe measurements of their electrical resistivities. A comparison of the temperature dependent resistivities of Ta_2S and Ta_3S_2 show that the latter compound is a considerably poorer conductor for all temperatures from 15 to 270 K, as predicted in our earlier band structure study of these materials and consistent with the recent work of Nozaki and coworkers. In both cases, resistivities were measured along the direction parallel to the $^1_\infty[Ta_3Ta]$ chains that serve as these materials' basic structural building blocks. The compounds $Ta_9M_2S_6$ (M = Fe, Co, Ni) show normal metallic behavior over the same range of temperatures. A distortion that leads to a doubling of the c-axis length for the Fe and Co containing compounds seems to have no significant effect on the electronic density of states at the Fermi level in either material. In contrast, the compounds $Ta_{11}M_2Se_8$ (M = Fe, Co, Ni) exhibit markedly different resistivities as a function of temperature. While $Ta_{11}Fe_2Se_8$ and $Ta_{11}Ni_2Se_8$ behave much like the structurally similar $Ta_9M_2S_6$ compounds, the resistivity of $Ta_{11}Co_2Se_8$ shows a curiously weak temperature dependence and a high residual value at the lowest temperatures of measurement (15 K). Powder diffraction data for this compound suggests that crystals prepared at low temperature have lower symmetry than the *Pnnm* space group originally reported.

Introduction, Structures, and Motivations

In recent years we have seen the synthesis of many novel binary and ternary Ta-rich chalcogenides, including several that are built up from chain-like building blocks. In the present paper we present the results of resistivity measurements for many of these compounds. We begin by describing some of the structural and theoretical motivations for this study. Both our structural and theoretical discussions will be brief; the reader is referred to original publications for more detail.

Harbrecht and Franzen reported the synthesis and structure of the $Ta_9M_2S_6$ (M = Fe, Co, Ni) compounds (*1*) with a subsequent structural reexamination that revealed 3*d*-metal pairing in the iron and cobalt containing compounds (*2*). Figure 1 shows a (001) projection of the $Ta_9M_2S_6$ (M = Fe, Co, Ni) structure in which only Ta–Ta bonds are depicted. The visually conspicuous building blocks of this structure are M-centered tricapped trigonal prisms, two of which occupy each cell in Fig. 1. These tetrakaidecahedra are fused on opposite triangular faces to form the chains shown on the left in Fig. 2. The Ta–Ta bonded framework is fully assembled when these chains are fused at the capping atoms to yield the extended network shown in Fig.

[1] To whom correspondence should be addressed.

0022-4596/93 $5.00

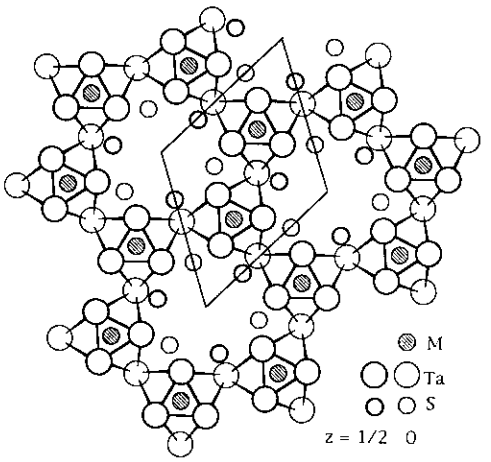

FIG. 1. (001) projection of the structure of $Ta_9M_2S_6$ (M = Fe, Co, and Ni).

1. While the overall connectivity of this structure is retained in the Fe and Co members of this series, these two compounds exhibit a distortion in which there is an apparent "pairing" of the 3*d* metal along the *c*-axis, as shown in Fig. 2. The alternation in Fe–Fe (Co–Co) distances is accompanied by an understandable alternating pattern of expanded and contracted Ta_3 triangles—short (long) Fe–Fe bonds intersect expanded (contracted) Ta_3 triangles. Calhorda and Hoffmann have studied the electronic structure of these materials, but were unable to arrive at any definitive conclusions regarding the driving force for the distortions observed in these two compounds (*3*). One of the objectives of the present study was to see whether the symmetry lowering might result in any change in the electrical transport properties of these materials.

A structurally related set of selenides, $Ta_{11}M_2Se_8$ (M = Fe, Co, Ni), were discovered in Harbrecht's laboratory, and share with the sulfides the characteristic structural motif of M-centered tricapped trigonal prismatic clusters condensed via triangular faces along the *c* direction—a (001) projection is shown in Fig. 3 (*4*). In this structure, the chains of tricapped trigonal prisms are fused to only one neighboring chain. (This fusion is illustrated in Fig. 4 and is similar to the fusion of chains in the $Ta_9M_2S_6$ series.) These double chains are more loosely coupled to neighboring double chains to complete the structure. (The sulfur and selenium coordination to the metal frameworks differ in the $Ta_9M_2S_6$ and $Ta_{11}M_2Se_8$ series; *1*, *2*, *4*.) Harbrecht reported some indication of disorder in the iron and cobalt containing $Ta_{11}M_2Se_8$ compounds, especially manifest in the 3*d*-element thermal parameters. However, crystals grown from melts in these systems did not exhibit long-range ordering with respect to distortions about the 3*d* metals. We have investigated these transport properties for all three derivatives.

More recently, we reported the single

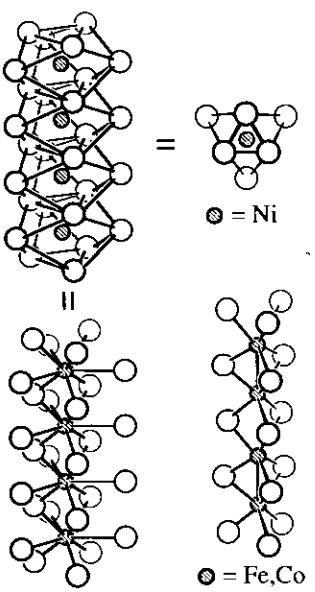

FIG. 2. M-centered tricapped trigonal prismatic chains of $Ta_9M_2S_6$ (M = Fe, Co, and Ni). A projection down-chain axis is shown at the upper right. At the upper- and lower-left, "sideviews" of the chains with Ta–Ta and Ta–M bonds are illustrated, respectively. At lower right, the core M-centered trigonal prisms are shown as they are found in the distorted Fe and Co compounds.

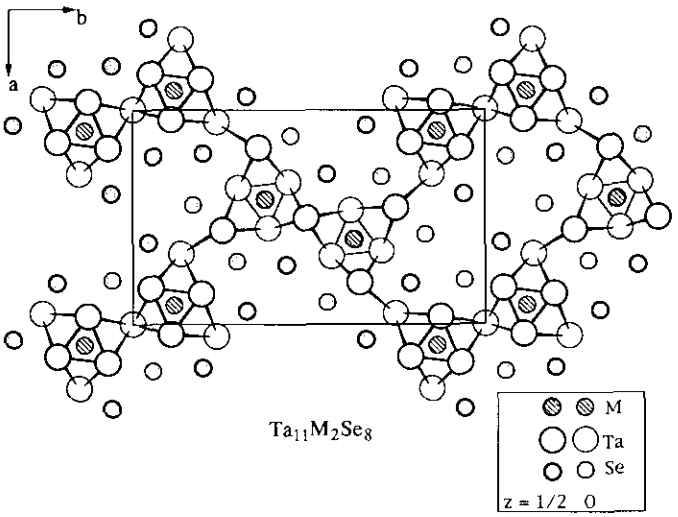

FIG. 3. (001) projection of the structure of $Ta_{11}M_2Se_8$ (M = Fe, Co, and Ni).

crystal structure of the binary sulfide Ta_3S_2 (*5–7*). The structure of this compound bears a close resemblance to Ta_2S, which was discovered in Franzen's laboratory more than twenty years ago (*8*). Both Ta_3S_2 and Ta_2S, like the more Ta-rich compound Ta_6S (*9, 10*), possess $^1_\infty$[Ta_5Ta] chains which may be described as infinite stacks of intergrown icosahedra (see Figs. 5 and 6). For our present purposes, the most important structural difference between the two compounds is the existence of a two-dimensional Ta–Ta bonded network in Ta_3S_2 and the cross linking of these 2D layers in Ta_2S to give a fully 3D network. Band structure calculations performed in our laboratories indicate that both compounds have optimal Ta–Ta bond-

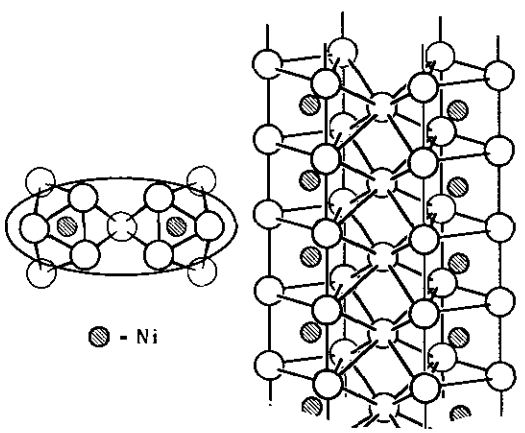

FIG. 4. The fusion of two chains of tricapped trigonal prisms in both of the structure types $Ta_9Ni_2S_6$ and $Ta_{11}Ni_2Se_8$. At left, the oval encloses that portion of the chains depicted in the view at right.

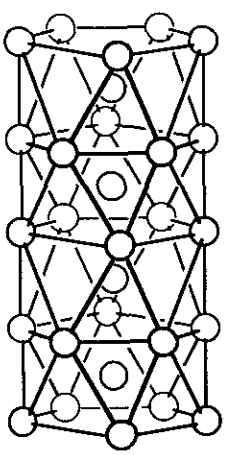

FIG. 5. The $^1_\infty$[Ta_5Ta] chain, a building block of Ta_3S_2, Ta_2S, and Ta_6S.

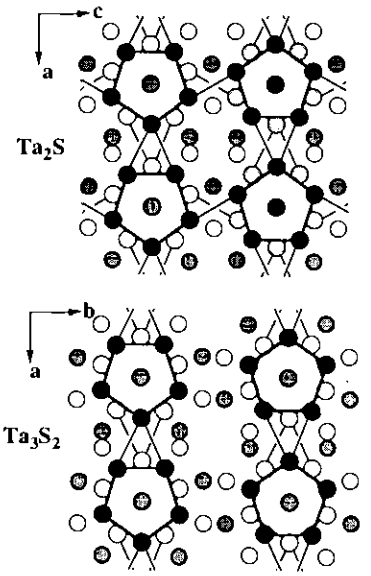

FIG. 6. The Ta_3S_2 and Ta_2S structure, projected on planes normal to the pentagonal antiprismatic chains [(001) for Ta_3S_2, (010) for Ta_2S]. Only Ta–Ta bonds within and between the pentagonal antiprisms are indicated.

ing (in that all crystal orbitals with Ta–Ta bonding character are occupied and levels with Ta–Ta antibonding character are vacant). Since in Ta_2S we have four electrons per Ta atom available for metal–metal bonding and in Ta_3S_2 we have 3.5 available electrons, the former compound has the electrons necessary to form the interlayer bonds illustrated in Fig. 6. The two DOS diagrams shown in Fig. 7 indicate that the increased dimensionality of the Ta–Ta bonded array has an especially important effect on the density of states at the Fermi level, $N(E_F)$. Using an extended Hückel tight-binding calculation we calculated a very small 0.09 eV band gap for the quasi-two-dimensional Ta_3S_2 (*6*). The method of computation is not of sufficient reliability for us to be confident of this result, but Ta_3S_2 is certainly predicted to have many fewer carriers than Ta_2S. The measurements in the present paper were performed to test this prediction.

The physical properties of these binary and ternary Ta-rich chalcogenides are unknown. In the present paper we report the results of single crystal conductivity measurements and discuss the properties observed with reference to the structural and theoretical expectations that have emerged in earlier work.

Experimental Methods

Sample preparation. Ta_3S_2 single crystals were grown in vapor phase transport reactions from TaS_2 and Ta. Reactions are run at 1000°C for two weeks with a trace of $TaBr_5$ used as a transport reagent. $Ta_9M_2S_6$ crystals were grown in a 950/900°C temperature gradient in vapor phase transport reactions using stoichiometric ratios of TaS_2, Ta, and M (M = Fe, Co, Ni) metal powders. $Ta_{11}M_2Se_8$ crystals are grown for two weeks in a 950/900°C temperature gradient in vapor phase transport reactions using stoichiometric ratios of $TaSe_2$, Ta, and metal powders (Fe, Co, Ni). $TaSe_2$ was prepared by reaction of the elements in a sealed silica vessel at 900°C (*4*). The transport reactions were carried out in sealed Ta capsules that were in turn encased in evacuated silica tubes. In preparing the selenides an inner wrapping

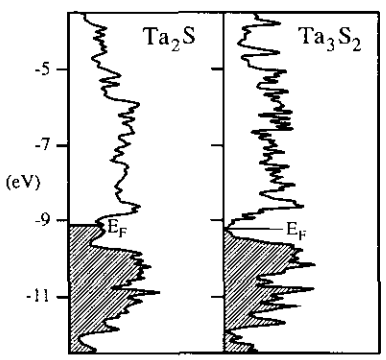

FIG. 7. Density of states (DOS) plots are shown for Ta_2S and Ta_3S_2. Shaded regions represent the occupied levels in each case (E_F indicates the Fermi energy).

of the Ta tube with Mo foil was used to reduce attack on the Ta tube. Ta_2S has been previously demonstrated to be a metastable phase that disproportionates at temperatures below 1300°C, so vapor phase transport synthesis of this compound is not feasible (*11*). It was therefore prepared from a melt starting with pressed pellets of powdered Ta and previously prepared TaS_2.

Characterization. Structures of the products were identified by X-ray diffraction measurement. X-ray powder diffraction patterns were obtained with a Enraf–Nonius (FR-552) vacuum Guinier camera using monochromated Cu $K\alpha_1$ radiation. Oscillation photographs with extended exposure times (±10°, 18 to 60 hr) were routinely taken on a Weissenberg camera both to verify that the chain axes corresponded with the *c*-axis (*b*-axis for Ta_2S) and to check for any obvious superlattice reflections. Under these conditions, the layer lines associated with *c*-axis doubling in $Ta_9M_2S_6$ (M = Fe, Co) are quite apparent (*2*). Crystals invariably exhibited an extreme rod-like habit with the needle axis collinear with the crystallographic *c*-axis.

For the computation of absolute resistivities, needle widths were measured with an optical microscope (×400) and for the smallest crystals with a Zeiss laser scan microscope (LSM-10). Crystal dimensions were 15 μm × 15 μm × 2 mm (Ta_3S_2), 7.3 μm × 7.3 μm × 1.5 mm ($Ta_9Fe_2S_6$), 4.5 μm × 9 μm × 1 mm ($Ta_9Co_2S_6$), 15.2 μm × 8.2 μm × 1 mm ($Ta_9Ni_2S_6$), 1.6 μm × 1.6 μm × 2 mm ($Ta_{11}Fe_2Se_8$), 1.7 μm × 1.7 μm × 1 mm ($Ta_{11}Co_2Se_8$), 3.8 μm × 3.8 μm × 1.5 mm ($Ta_{11}Ni_2Se_8$). Dimensions of the Ta_2S crystal were 0.15 × 0.003 × 0.013 cm^3. Micrographs shown in Fig. 8 were obtained using a scanning electron microscope (JEOL 6400).

Electrical resistivity measurements. Resistivities were measured by the four-probe method using single crystals for all compounds (except Ta_2S). A locally prepared In–Ga (1 : 1) solder was used to make all contacts to crystals; leads from these contacts were made with 0.1 mm diameter gold wire. For each compound, temperature dependent measurements for the range 15 to 273 K were repeated at least twice on separate crystals. Independent measurements between 77 and 273 K were performed on at least six different crystals for each compound (twice for Ta_2S). Reproducibility of the temperature dependence of the resistivities was generally excellent. All absolute resistivities were reproducible with better than 10% precision. Except for intrinsic defects that are beyond our control, the factor that is most important in limiting the accuracy of our measurements seems to be the accuracy with which we are able to measure the cross-sectional areas of the crystals used in measurements. Resistivity data for Ta_2S are reported for measurements carried out with two different polycrystalline samples. Using a crushed pellet sample, pieces were isolated for which both chain axis (*b*-axis) alignment and sample size were deemed to be acceptable for subsequent measurements.

Magnetic susceptibilities. The susceptibilities of powder samples with typical mass of 75 mg were determined with a George Associates force magnetometer. Samples were contained in carefully dried capsules (Kel-F), the susceptibilities of which were measured in separate runs and corrected for diamagnetic contributions.

Results and Discussion

Every compound for which we report measurements was originally synthesized at high temperature, in either an arc-melting reaction or from a reaction in an induction furnace. In contrast, we obtain single crystals of Ta_3S_2, $Ta_9M_2S_6$ (M = Fe, Co, Ni), and $Ta_{11}M_2Se_8$ (M = Fe, Co, Ni) from vapor phase transport reactions. Typically, reactions are performed in a 950/900°C tempera-

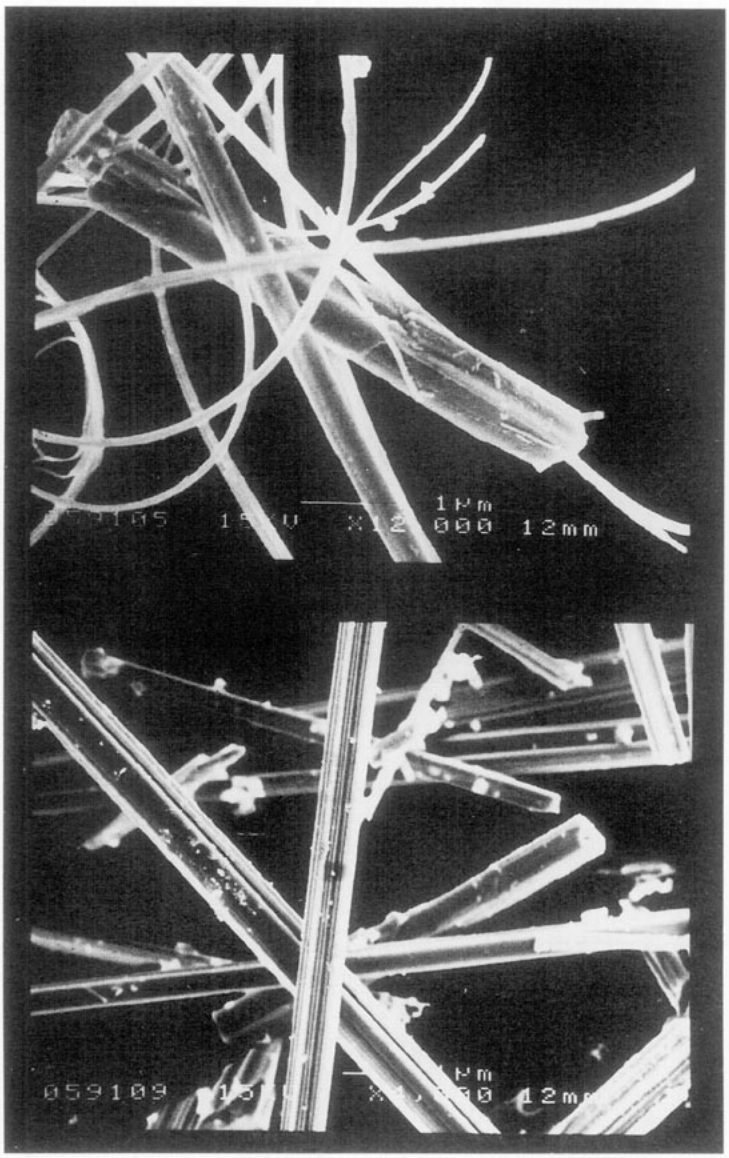

FIG. 8. Scanning electron micrographs of Ta_3S_2 and $Ta_9Fe_2S_6$.

ture gradient and products form at the hot end of the reaction tube. We use stoichiometric mixtures of Ta powder, TaS_2 (or $TaSe_2$), and powdered metal M (where appropriate), with a trace of $TaBr_5$ as a transport agent. Each of these compounds forms crystals that are very anisotropic fibers, with thicknesses from 0.5 to 10 μm and lengths of up to 1 cm. Scanning electron micrographs of Ta_3S_2 and $Ta_9Fe_2S_6$ shown in Fig. 8 give some indication of the appearance of these crystals.

Extended exposure oscillation photographs indicated that the fiber axis was coin-

cident with the crystallographic c-axis (and the appropriate chain axis) in all compounds studied. In each case, powder diffraction patterns obtained by selecting samples of these fibrous crystals show no sign of any compounds but the intended product. This is true even in the preparation of Ta_3S_2, where reaction with the walls of the Ta tube might have been expected to yield some of the more metal-rich phases Ta_2S or Ta_6S. But Ta_2S is not thermodynamically stable at these temperatures, and if Ta_6S is formed it remains imbedded in the tube walls (*11, 12*). Each of these compounds is sufficiently air stable that In/Ga alloy contacts can be applied in air. The sulfides seem to show some modest surface oxidation over a period of months when stored in a desiccator; the selenides show somewhat more degradation over the same period.

The room temperature resistivities of the compounds studied fall in the range from 200 to 4000 $\mu\Omega$-cm, with Ta_2S being the best conductor and $Ta_{11}Co_2Se_8$ being the poorest. Except for Ta_2S, these resistivities are somewhat larger than typical transition metal compounds, though not inordinately so. For comparison, we note that the ternary molybdenum chalcogenides $M^IMo_3Se_3$ (M^I = K, Rb, Cs, Tl) show room-temperature resistivities ranging from 150 to 400 $\mu\Omega$-cm (*13*).

The magnetic susceptibilities of $Ta_9M_2S_6$ (M = Co and Ni) are small and virtually temperature independent from 77 to 273 K, with no indication that there is any local magnetic moment associated with the Co or Ni centers in these materials. Unfortunately, susceptibility measurements on $Ta_9Fe_2S_6$ are not reproducible ($\approx 10^{-3}$ emu/mole), probably indicating the presence of ferromagnetic impurities (perhaps elemental iron).

In Fig. 9, we show the temperature dependence of the resistivity of Ta_3S_2 and Ta_2S, the former measured from 15 to 273 K, the latter from 86 to 273 K. Because of its low

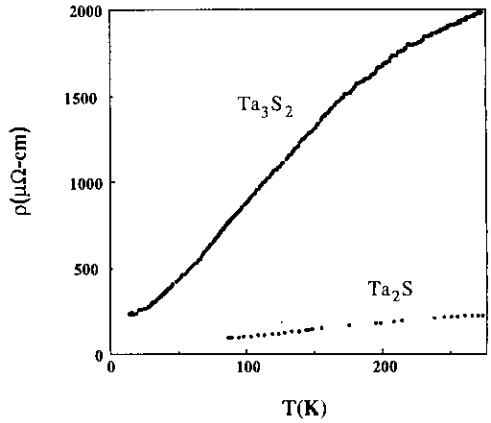

FIG. 9. Temperature dependence of the single-crystal dc resistivities of Ta_3S_2 and Ta_2S.

temperature instability, single crystals of Ta_2S cannot be grown as those for the other materials studied. The data shown for this compound are for a thin rod-like chip collected from a shattered arc-melted button. This chip shows a clean, well-layered oscillation photo indicating that the long axis is collinear with the $\frac{1}{\infty}$[Ta_5Ta] chains (the [010] direction in this case). Still, the sample may consist of more than one mutually aligned crystal. Data for Ta_3S_2 are for a single crystal, as described above.

The meaning of the data in Fig. 9 is clear. Both Ta_3S_2 and Ta_2S behave as conductors, with resistivity increasing with temperature. However, for all temperatures, the resistivity of Ta_2S is an order of magnitude smaller than that of Ta_3S_2. We believe this to be an intrinsic effect. There is every reason to believe that the crystals available for Ta_3S_2 are at least as free from defects as those for Ta_2S since the former were grown at relatively low temperature while Ta_2S samples were rapidly quenched from the melt. Then the most reasonable interpretation of the resistivity data is that suggested by Fig. 7: the density of states at the Fermi level is much lower for Ta_3S_2. Nozaki and coworkers have recently carried out a more thorough galvanomagnetic study on Ta_3S_2, Ta_2S, and Ta_6S using polycrystalline sam-

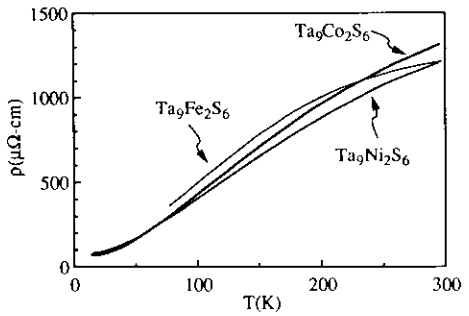

FIG. 10. Temperature dependence of the single-crystal dc resistivities of $Ta_9M_2S_6$ (M = Fe, Co, and Ni).

ples (*14*). Their results are in good agreement with those reported here and strongly confirm our theoretical picture of the electronic structure of these materials. We have so far been unable to realize a synthetic goal that is an even better test of the theory—materials in which isolated $^1_\infty[Ta_5TaS_5]$ chains occur (free from interchain Ta–Ta bonds). For the appropriate (optimal) number of electrons for bonding within these chains, we have predicted semiconducting behavior (*6*).

The temperature dependence of the resistivity for the series of compounds $Ta_9M_2S_6$ (M = Fe, Co, Ni) is shown in Fig. 10; data for the Co and Ni compounds over the temperature range from 15 to 300 K, those for the Fe compound range from 77 to 300 K. The curves are clearly similar and indicative of simple metallic behavior. If there are any surprises here, it is that the distorted Fe and Co compounds show no qualitative difference with the undistorted Ni compound. We might have expected that the chain distortions illustrated in Fig. 2 are driven by an electronic instability. Generally the result of such a distortion is the opening of a band gap, or at least one expects that the distortion may create a local minimum in the DOS. However, to the extent that we can assume that carrier mobilities should be similar in these three materials, $N(E_F)$ must also be similar.

The compounds $Ta_{11}M_2Se_8$ (M = Fe, Co, Ni) show more dissimilar behavior; resistivities are plotted in Fig. 11. $Ta_{11}Fe_2Se_8$ and $Ta_{11}Ni_2Se_8$ behave much like the $Ta_9M_2S_6$ compounds already discussed, while $Ta_{11}Co_2Se_8$ is a poorer conductor than even Ta_3S_2 and exhibits a marked resistivity (> 2 $\mu\Omega$-cm) even at the lowest temperatures. As one approaches room temperature from below, the resistivity shows a very slight decrease. This behavior is quite reproducible and it as such seems unlikely to be associated with the contacts between the In/Ga alloy and the crystal surface. (In any case, it is quite likely that any reactions that occurred at this interface would also occur for the Fe and Ni analogues.) Measurements at temperatures above room temperature are anticipated.

Powder diffraction data show some distinct splitting of lines in $Ta_{11}Co_2Se_8$ when compared with the pattern obtained for this compound when prepared in an arc-melting reaction, or when compared with $Ta_{11}M_2Se_8$ (M = Fe, Ni) prepared either by vapor phase transport synthesis or by arc melting. In particular, the (002) line is broadened when either of these compounds is prepared by arc-melting and is split into a distinct pair of lines in $Ta_{11}Co_2Se_8$ prepared by vapor phase transport. The splitting of this line

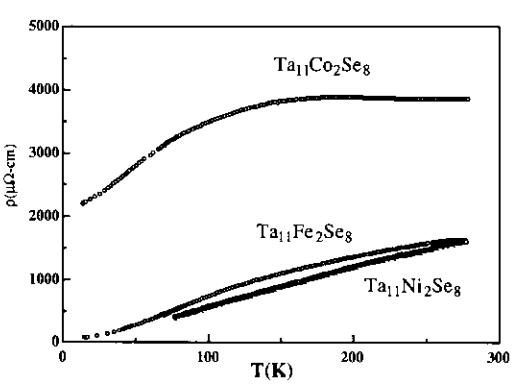

FIG. 11. Temperature dependence of the single-crystal dc resistivities of $Ta_{11}M_2Se_8$ (M = Fe, Co, and Ni).

seems incompatible with an orthorhombic space group for this compound. We are presently reexamining the $Ta_{11}Co_2Se_8$ structure to determine whether the structural distortions alluded to in Harbrecht's original report exhibit long-range order in crystals grown by vapor phase transport. At present, the differences do not seem to involve a mere difference in temperature from which the samples are quenched. When samples of $Ta_{11}Co_2Se_8$ prepared by arc-melting are annealed for 2 days at 950°C, the powder diffraction pattern is unchanged when compared with that for a sample quenched from the melt.

Concluding Remarks

Our intuitive expectation of metallic behavior for metal-rich compounds must be somewhat modified when dealing with materials like Ta_3S_2 and especially $Ta_{11}Co_2Se_8$. The existence of unbroken and undistorted chains of metal–metal bonds does not seem to guarantee metallic behavior. While Ta_3S_2 is metallic, the rather poor conductivity we find herein (compared with a suitable structural analogue like Ta_2S) indicates that the density of states at the Fermi level is small. Our single crystal results are consistent with those of Nozaki and coworkers (*14*). With $Ta_{11}Co_2Se_8$ the situation is still unclear and we are now attempting to discover whether a structural distortion in this material is correlated with its odd resistivity behavior.

Acknowledgments

We gratefully acknowledge the support of the National Science Foundation for its support through a Presidential Young Investigator Award (Grant DMR-8858151) and the Robert A. Welch Foundation for its support through Grant A-1132. We thank James Long in the Center for Electron Microscopy at Texas A&M for providing his expertise and Professor R. K. Pandey in the Department of Electrical Engineering at Texas A&M for generous use of the conductivity apparatus employed in low temperature measurements. We also thank Charles Runyan for his assistance in performing the magnetic susceptibility measurements.

References

1. B. Harbrecht and H. F. Franzen, *J. Less-Common Met.* **113,** 349 (1985).
2. B. Harbrecht, *J. Less-Common Met.* **124,** 125 (1986).
3. M. J. Calhorda and R. Hoffmann, *Inorg. Chem.* **27,** 4679 (1988).
4. B. Harbrecht, *J. Less-Common Met.* **141,** 59 (1988).
5. T. Hughbanks, *Prog. Solid State Chem.* **19,** 329 (1989).
6. S.-J. Kim, K. S. Nanjundaswamy, and T. Hughbanks, *Inorg. Chem.* **30,** 159 (1991).
7. H. Wada and M. Onoda, *Mater. Res. Bull.* **24,** 191 (1989).
8. H. F. Franzen and J. G. Smeggil, *Acta Crystallogr. Sect. B* **25,** 1736 (1969).
9. H. F. Franzen and J. G. Smeggil, *Acta Crystallogr. Sect. B* **26,** 125 (1970).
10. B. Harbrecht, *J. Less-Common Met.* **138,** 225 (1988).
11. K. S. Nanjundaswamy and T. Hughbanks, *J. Solid State Chem.* **98,** 278 (1992).
12. B. Harbrecht, S. R. Schmidt, and H. F. Franzen, *J. Solid State Chem.* **53,** 113 (1984).
13. J. M. Tarascon, F. J. DiSalvo, and J. V. Waszczak, *Solid State Commun.* **52,** 227 (1984).
14. H. Nozaki, H. Wada, and S. Takekawa, *J. Phys. Soc. Jpn.* **60,** 3510 (1991).